Inviscid Transient Growth on Horizontal Shear Layers with Strong Vertical Stratification

Cristóbal Arratia, Sabine Ortiz and Jean-Marc Chomaz

Abstract We report an investigation of the three-dimensional stability of an horizontal free shear layer in an inviscid fluid with strong, vertical and constant density stratification. We compute the optimal perturbations for different optimization times and wavenumbers. The results allow comparing the potential for perturbation energy amplification of the free shear layer instability and the different mechanisms of transient growth. We quantify the internal wave energy content of the perturbations and identify different types of optimal perturbations. Intense excitation of gravity waves due to transient growth of perturbations is found in a broad region of the wavevector plane. Those gravity waves are eventually emitted away from the shear layer.

1 Introduction

During the last years, there has been an increased interest in the effects of horizontal shear in geophysical flows. In that context, a horizontal mixing layer with vertical stratification is one idealized flow model presenting the effect of shear and also the free shear or Kelvin-Helmholtz (KH) instability. The two dimensional (2D) modes of the KH instability are not affected by stratification. The vertical structure developing in such a flow is however strongly affected by stratification, as shown by the direct

C. Arratia (✉)
Departamento de Física FCFM, Universidad de Chile, Blanco Encalada 2008, Santiago, Chile
e-mail: cristobal.arratia@gmail.com

C. Arratia · S. Ortiz · J.-M. Chomaz
LadHyX, CNRS-École Polytechnique, 91128 Palaiseau Cedex, France

S. Ortiz
e-mail: ortiz@ladhyx.polytechnique.fr

J.-M. Chomaz
e-mail: chomaz@ladhyx.polytechnique.fr

S. Ortiz
UME/DFA, ENSTA, Chemin de la Hunière, 91761 Palaiseau Cedex, France

M. Tlidi and M.G. Clerc (eds.), *Nonlinear Dynamics: Materials, Theory and Experiments*, Springer Proceedings in Physics 173,
DOI 10.1007/978-3-319-24871-4_15

numerical simulations (DNS) performed by Basak and Sarkar [7]. They show the appearance of a layered structure consisting of a stack of 'pancake' vortices with a vertical correlation length of the order of the buoyancy length. Despite the non applicability of Squire's theorem to this flow, it has been shown in [10] that the most unstable mode is still 2D. This implies that modal stability analysis on the parallel shear layer does not select a specific vertical lengthscale. For strong stratification, however, the range of unstable vertical wavenumbers widens proportionally to the inverse of the Froude number, which means that stronger stratification destabilizes smaller vertical lengthscales [10]. This is a consequence of the self-similarity of strongly stratified inviscid flows found by Billant and Chomaz [8].

Another important aspect of horizontal shear flows with vertical stratification concerns internal gravity wave generation and emission. The generation and emission of internal waves has been studied, among others, by Vanneste and Yavneh [12] in the rotating case and by Bakas and Farrell [6] in the non-rotating case. Both studies focus on linearized dynamics of perturbations of plane constant shear flow, which allows finding analytic expressions for the generated wave amplitude in different asymptotic regimes. This simplified model has no unstable modes nor intrinsic horizontal lengthscale.

Here we consider linearized perturbations of a horizontal mixing layer with a tanh velocity profile and vertical stratification on a non-rotating frame. We study the sensitivity to initial conditions by computing the optimal perturbations, which are those that maximize the energy growth up to an optimization time T. We compute the optimal perturbations for a broad range of streamwise and spanwise wavenumbers and for different optimization times T. In this way we can determine, for different times, whether the KH instabilty or other transient growth mechanisms are more efficient in extracting energy from the basic flow. We then quantify the vortex and gravity wave energy content of the perturbations by means of a Craya-Herring, or poloidal-toroidal, decomposition [11]. This decomposition helps identifying different types of optimal perturbations according to their wave/vortex energy content. We show that some of the optimal perturbations involve the generation of waves that are eventually radiated away from the shear layer.

2 Formulation and Methods

We consider the evolution of the perturbative velocity $\mathbf{u}(\mathbf{x}, t)$ and density $\rho(\mathbf{x}, t)$ fields according to the linearized incompressible Euler equations in the Boussinesq approximation. Here $\mathbf{x} = (x, y, z)$ is the cartesian coordinate vector with z increasing upwards, and t is the time coordinate. Our base state is $\mathbf{U} = \tanh(y)\mathbf{e}_x$ with a stable linear density stratification $\rho_B(z) = \rho_0(1 - N^2 z/g)$, where ρ_0 is a reference density, g is the acceleration of gravity and $N = \sqrt{-g/\rho_0 d\rho_B/dz}$ is the Brunt-Väisälä frequency. With this variables, the horizontal Froude number corresponding to the ratio between the buoyancy and advective time scales is $F_h = N^{-1}$.

Linearity and homogeneity in x and z of the evolution equations allow us to rewrite the fields as $[\mathbf{u}, \rho](x, y, z, t) \longrightarrow [\mathbf{u}, \rho](y, t)e^{i(k_x x + k_z z)}$, and to consider independently the evolution of the different streamwise-spanwise wavenumbers. Because of the latter, for each point in the (k_x, k_z)-plane we can define the optimal gain as

$$G(T) = \max_{[\mathbf{u},\rho](y,0)} \left(\frac{E(T)}{E(0)} \right), \tag{1}$$

where the total energy E is given up to a constant by

$$E = \int \left(\mathbf{u}^2 + N^2 \rho^2 \right) \mathrm{d}y. \tag{2}$$

Thus, $G(T)$ is the maximum attainable increase in energy up to the optimization time T. We span the (k_x, k_z)-plane for each time T at which we compute the optimal perturbation. We characterize the transient growth by the optimal mean growth rate of the perturbation

$$\sigma_m(k_x, k_z, T) = \frac{1}{2T} \int_0^T \frac{\partial}{\partial t} \log \left[E(k_x, k_z, t) \right] \mathrm{d}t, \tag{3}$$

where $E(k_x, k_z, t)$ is the energy of the optimal perturbation. Using definition (3) we can directly compare the amplification of the optimal perturbations with the growth rate of the most unstable KH mode, $\sigma_{KH} = 0.1897$ [10].

The optimal perturbations are computed by the iterative procedure described in [9], whereby the succesive numerical integration of the direct and the time reversed adjoint equations is performed until convergence is achieved. The adjoint equations and optimization algorithm have been adapted on a pseudo-spectral DNS code, same as in [3].

Throughout this paper we will use $F_h = 0.1$, which is small enough so that the strongly stratified similarity described in [8] holds to a very good approximation [2], as is also the case for the eigenmodes [10] and for the viscous transient growth after correcting by the viscous damping factor $e^{\nu k_z^2 T}$, where ν is the viscosity [4]. In this context, the main consequence of this scaling law is that, for $F_h \lesssim 0.1$, we can plot the results as a function of $k_z F_h$ to capture the dependence on both k_z and F_h. The results are not significantly different for $F_h < 1$ [2].

3 Results

Figure 1 shows $\sigma_m(k_x, F_h k_z)$ for $T = 4, 7, 10$ and 15. The colorbars indicate that σ_m decreases as T increases. The dashed line on each of the figures indicates roughly the ratio $r = F_h k_z / k_x$ at which the optimal perturbations are less amplified. The value of r corresponding to the dashed lines, say r_{min}, increases as T increases. For

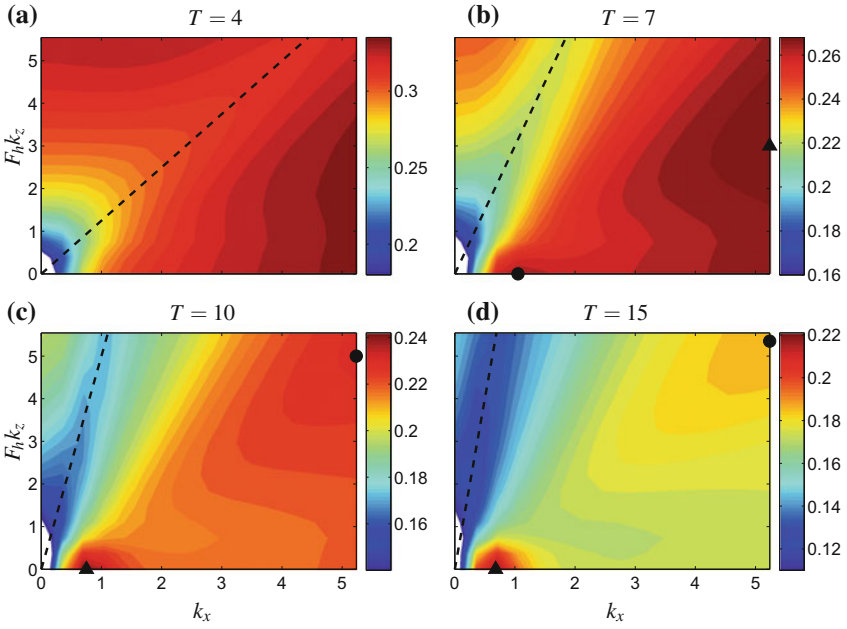

Fig. 1 Optimal mean growth rate $\sigma_m(k_x, F_h k_z)$ for optimization times $T = 4$ (**a**), $T = 7$ (**b**), $T = 10$ (**c**), and $T = 15$ (**d**). The *colorbar* is indicated next to each figure. The *horizontal* and *vertical axis* are the same on all figures, as shown in the *lower left figure* (**c**). The values of the ratio $F_h k_z / k_x$ indicated by the *dashed lines* are $r_{min} = 5/4, 3, 5$ and 8 for $T = 4, 7, 10$ and 15, respectively. In (**b**–**d**), the ▲ indicates the maximum of the computed σ_m (at the boundary in **c**) and the • indicates a secondary local maximum (at the boundary in **c** and **d**)

$T = 4$, σ_m increases as $k = \sqrt{k_x^2 + (F_h k_z)^2}$ increases and shows no clear maximum. For $T = 7$, 10 and 15, the global maximum of the computed σ_m is indicated by a ▲ and a second, local maximum of the computed σ_m is marked by a •; these are located at large k and around the KH unstable region with $k_z = 0$. For $T = 7$, the maximum occurs for large k at the ▲ around $r = 3/5$, and the maximum close to the KH unstable region is only a local maximum. For $T = 10$ and 15, the global maximum is 2D and located in the KH unstable region, while the secondary maximum appears at large k, at the boundary of the domain.

3.1 Craya-Herring Decomposition

Following [11], we define the Craya-Herring basis $(\mathbf{e}_1, \mathbf{e}_2, \mathbf{e}_3)$ as $\mathbf{e}_1 = \mathbf{k} \times \mathbf{e}_z / |\mathbf{k} \times \mathbf{e}_z|$, $\mathbf{e}_2 = \mathbf{k} \times (\mathbf{k} \times \mathbf{e}_z) / |\mathbf{k} \times (\mathbf{k} \times \mathbf{e}_z)|$ and $\mathbf{e}_3 = \mathbf{k}/|\mathbf{k}|$, where $\mathbf{k} = (k_x, k_y, k_z)^T$ is the wave vector. In this orthonormal basis, the Fourier transform of the velocity field becomes $\hat{\mathbf{u}} = \hat{\phi}_1 \mathbf{e}_1 + \hat{\phi}_2 \mathbf{e}_2$ because $\hat{\mathbf{u}} \cdot \mathbf{e}_3 = 0$ due to the incompressibility condition.

When $\sqrt{k_x^2 + k_y^2} \neq 0$, the energy density in spectral space $\varepsilon(\mathbf{k})$ is given by

$$\varepsilon(\mathbf{k}) = |\hat{\phi}_1|^2 + |\hat{\phi}_2|^2 + |\hat{\phi}_3|^2, \tag{4}$$

with

$$\hat{\phi}_1 = \frac{i}{\sqrt{k_x^2 + k_y^2}} \hat{\omega}_z, \tag{5a}$$

$$\hat{\phi}_2 = -\sqrt{\frac{k_x^2 + k_y^2 + k_z^2}{k_x^2 + k_y^2}} \hat{u}_z, \tag{5b}$$

$$\hat{\phi}_3 = N\hat{\rho}, \tag{5c}$$

where $\hat{\omega}_z$ is the Fourier transformed vertical vorticity. The total energy may be expressed as $E = \int \varepsilon \, \mathrm{d}k_x \mathrm{d}k_y \mathrm{d}k_z$.

The $\hat{\phi}_1 \mathbf{e}_1$ part of the velocity field is purely horizontal so it does not directly affect the disturbance density field. For the linear dynamics in the absence of a basic flow, decomposition (5) provides a separation of the fields in which the $\hat{\phi}_1 \mathbf{e}_1$ part of the velocity field decouples from the internal wave dynamics given by $\hat{\phi}_2$ and $\hat{\phi}_3$. Despite the fact that the wave and vortical parts of the velocity field can not be unambiguously split in a general case, this decomposition provides an objective, physically motivated way of quantifying the wave content of the perturbative field. We will thus refer to the different components as the wave and vortex parts of the flow fields.

Figure 2 shows the fraction of the total energy contained in the vortex part $\hat{\phi}_1$ of the velocity field, for each of the optimal perturbations of Fig. 1. Figure 2 shows the energy fractions of the optimal initial condition ($t = 0$) and the optimal response ($t = T$). Also shown are the dashed lines of Fig. 1 indicating r_{min}, the value of $r = F_h k_z / k_x$ where the optimal perturbations have lower growth. Blue contours indicate that most of the perturbation energy corresponds to gravity waves. In the left column we observe that the wave content of the optimal initial condition depends mainly on r. The energy of the optimal initial condition is given by the vortex part for $r = 0$ and the energy of the wave part becomes increasingly important as r increases. It can be seen that the dashed lines at r_{min} coincide, roughly but consistently for all T, with the region where the energy of the optimal initial condition changes from being mostly vortex to mostly wave. The energy of the optimal response, on the other hand, is mostly given by the vortex part for $k_x \sim 0$ and for $F_h k_z \sim 0$, while for most of the domain where k_x, $F_h k_z \gtrsim 1$, the energy of the optimal response is mainly in the wave part.

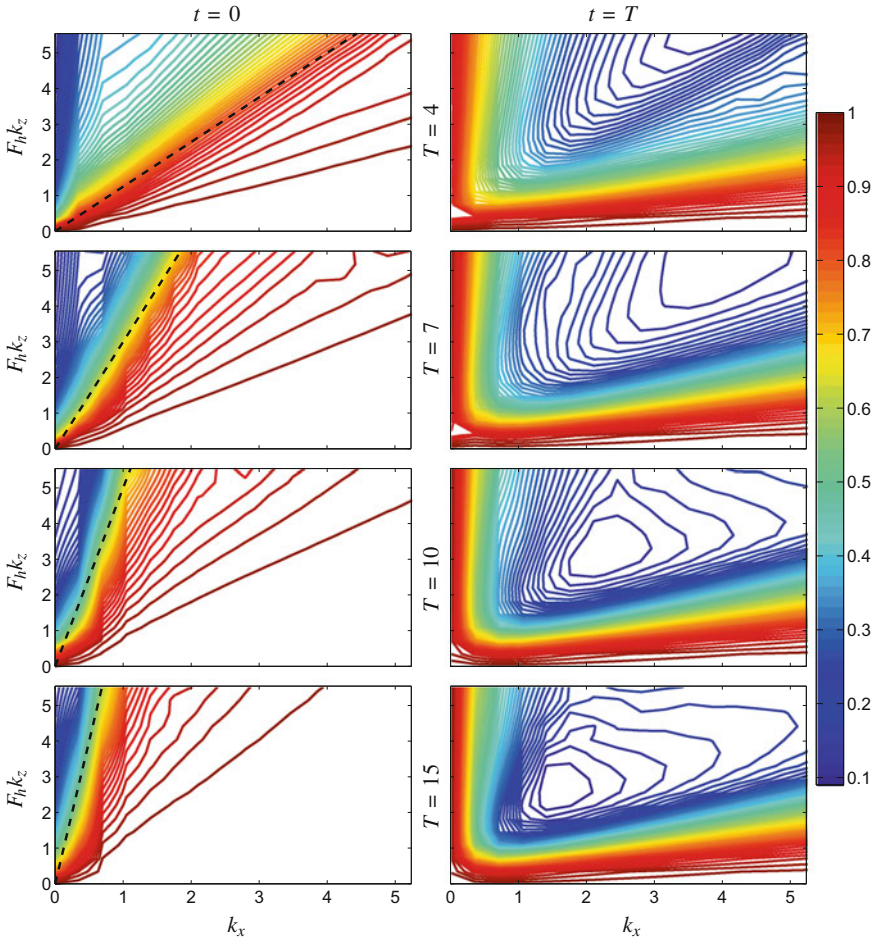

Fig. 2 Energy fraction in the vortical part $\frac{\int |\hat{\phi}_1|^2 \, \mathrm{d}k_y}{E}$ for the optimal perturbations at $t = 0$ (*left column*) and optimal response at $t = T$ (*right column*). The optimization time for each row, starting from above, are $T = 4$, $T = 7$, $T = 10$ and $T = 15$, as indicated on the figure. Here, for $k_x = 0$, the energy of the horizontal mean flow (which corresponds to $\sqrt{k_x^2 + k_y^2} = 0$) has been added to the energy of $\hat{\phi}_1$

4 Discussion

Figures 1 and 2 help in distiguishing three main regions on the $(k_x, F_h k_z)$ plane. First, for $F_h k_z \sim 0$, the dynamics is dominated by the vertical vorticity (Fig. 2) and is essentially 2D. In this region, the Orr mechanism dominates the inviscid transient growth for short time (Fig. 1a) and for large k_x, while the KH instability becomes increasingly important as T increases (Fig. 1b–d). Second, for $k_x \sim 0$, the optimal

transient growth consists of waves generating large horizontal velocity (Fig. 2), giving large transient growth for short times (Fig. 1a, b). The mechanism involved here is the transient generation of streamwise streaks during the passage of waves through shear [2, 5]. This transient growth mechanism is similar to the lift-up mechanism, it produces streamwise velocity as a result of cross-stream transport. This mechanism is perhaps related to the cross-stream transport of KH billows that is linked to the layered structure reported in [7], see also [1]. Third, for k_x, $F_h k_z \gtrsim 1$ and $r \lesssim r_{min}$, the optimal perturbations result mainly in the generation of wave energy from the vortical part (Fig. 2). This is an efficient mechanism of perturbation energy growth, the most efficient indeed for intermediate times ($T = 7$ in Fig. 1b). In the absence of viscosity, this mechanism does not seem to reach a maximum of σ_m for finite (k_x, k_z).

An important aspect concerns whether the generated wave energy remains in the wave part after T. Figure 3 shows spatio-temporal diagrams of the vortex and wave energy density for an optimal perturbation at $T = 7$, for (k_x, k_z) in the region of wave generation and largest energy growth (close to the ▲ in Fig. 1b). From $t = 0$ to 7, the perturbation energy grows by a factor of 43.6, more than any unstable mode during that time. Initially, most of the energy growth occurs on the vortical part. Wave energy starts being noticeable around $t = 5$ and then increases quickly when the vortex energy is transferred into the wave part of the flow. The generated wave is then radiated away after the optimization time. This qualitative behaviour is the same for different optimization times.

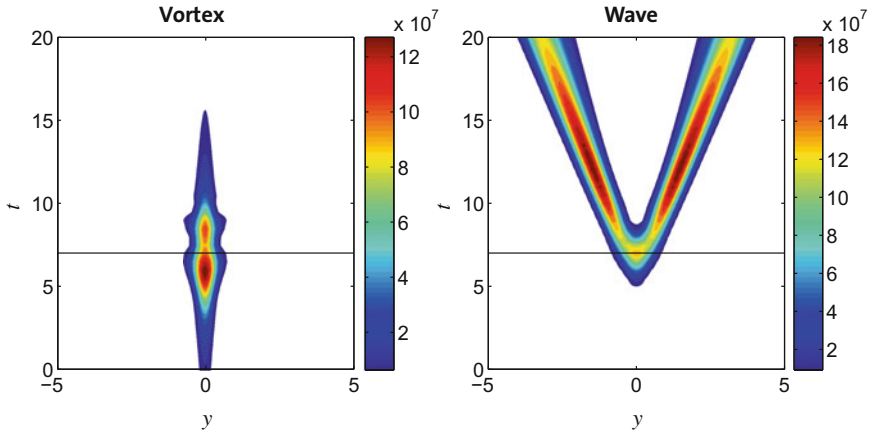

Fig. 3 Spatio-temporal diagram of the optimal perturbation for $T = 7$ (*horizontal line*), $(k_x, F_h k_z) = (4.89, 2.96)$. *Colorbar* shows the energy density of the vortex (*left*) and internal gravity wave (*right*) components of the flow. The vortex energy density is obtained by taking the inverse Fourier transform in the y direction of $|\hat{\phi}_1|^2$ evaluated at the corresponding (k_x, k_z). The same is done with $|\hat{\phi}_2|^2 + |\hat{\phi}_3|^2$ for the energy of the wave part

5 Conclusion

We have computed the optimal perturbations on a horizontal mixing layer with strong vertical stratification. For short optimization times (up to T between 7 and 10), the most amplified perturbations occur for large wavenumbers, away from the KH unstable region that dominates for large T. We have done a Craya-Herring decomposition to quantify the wave and vortex energy content of the optimal perturbations. Using this decomposition we can distinguish 3 main different types of optimal perturbations: quasi 2D for $F_h k_z \sim 0$, streamwise streaks generated by waves for $k_x \sim 0$, and waves generated by vortical motion for k_x, $F_h k_z \gtrsim 1$ and $r \lesssim r_{min}$.

An important result is the fact that, for moderate times ($T \sim 7$), the most amplified optimal perturbations produce waves that are eventually radiated away from the shear layer. This wave generation and emission mechanism remains efficient in the large wavenumber region even for larger T, when the KH instability becomes the most efficient mechanism.

References

1. E. Arobone, S. Sarkar, The statistical evolution of a stratified mixing layer with horizontal shear invoking feature extraction. Phys. Fluids **22**(11), 115108 (2010)
2. C. Arratia, Non-modal instability mechanisms in stratified and homogeneous shear flows. PhD Thesis, Ecole Polytechnique (2011). http://tel.archives-ouvertes.fr/pastel-00672072/
3. C. Arratia, C.P. Caulfield, J.-M. Chomaz, Transient perturbation growth in time-dependent mixing layers. J. Fluid Mech. **717**(1), 90–133 (2013)
4. C. Arratia, S. Ortiz, J.M. Chomaz, Transient evolution and high stratification scaling in horizontal mixing layers, in *Advances in Turbulence XII*, ed. by B. Eckhardt, pp. 183–186. Springer, Heidelberg (2009)
5. N.A. Bakas, B.F. Farrell, Gravity waves in a horizontal shear flow. Part I: growth mechanisms in the absence of potential vorticity perturbations. J. Phys. Oceanogr. **39**(3), 481–496 (2009a)
6. N.A. Bakas, B.F. Farrell, Gravity waves in a horizontal shear flow. Part II: interaction between gravity waves and potential vorticity perturbations. J. Phys. Oceanogr. **39**(3), 497–511 (2009b)
7. S. Basak, S. Sarkar, Dynamics of a stratified shear layer with horizontal shear. J. Fluid Mech. **568**(1), 19–54 (2006)
8. P. Billant, J.-M. Chomaz, Self-similarity of strongly stratified inviscid flows. Phys. Fluids **13**(6), 1645–1651 (2001)
9. P. Corbett, A. Bottaro, Optimal linear growth in swept boundary layers. J. Fluid Mech. **435**(1), 1–23 (2001)
10. A. Deloncle, J.-M. Chomaz, P. Billant, Three-dimensional stability of a horizontally sheared flow in a stably stratified fluid. J. Fluid Mech. **570**(1), 297–305 (2007)
11. F.S. Godeferd, C. Cambon, Detailed investigation of energy transfers in homogeneous stratified turbulence. Phys. Fluids **6**(6), 2084–2100 (1994)
12. J. Vanneste, I. Yavneh, Exponentially small inertia-gravity waves and the breakdown of quasi-geostrophic balance. J. Atmos. Sci. **61**(2), 211–223 (2004)